



HAL
open science

Fluorescently Labeled Branched Copolymer Nanoparticles for In Situ Characterization of Nanovectors and Imaging of Cargo Release

Sophie Bou, Andrey S Klymchenko, Mayeul Collot

► **To cite this version:**

Sophie Bou, Andrey S Klymchenko, Mayeul Collot. Fluorescently Labeled Branched Copolymer Nanoparticles for In Situ Characterization of Nanovectors and Imaging of Cargo Release. ACS Applied Nano Materials, 2022, 5 (3), pp.4241 - 4251. 10.1021/acsanm.1c04582 . hal-03842777

HAL Id: hal-03842777

<https://hal.science/hal-03842777>

Submitted on 7 Nov 2022

HAL is a multi-disciplinary open access archive for the deposit and dissemination of scientific research documents, whether they are published or not. The documents may come from teaching and research institutions in France or abroad, or from public or private research centers.

L'archive ouverte pluridisciplinaire **HAL**, est destinée au dépôt et à la diffusion de documents scientifiques de niveau recherche, publiés ou non, émanant des établissements d'enseignement et de recherche français ou étrangers, des laboratoires publics ou privés.

Fluorescently-Labeled Branched Copolymers Nanoparticles for In Situ Characterization of Nanovectors and Imaging of Cargo Release

Sophie Bou,¹ Andrey S. Klymchenko,¹ Mayeul Collot^{1*}

¹Laboratoire de Bioimagerie et Pathologies, UMR 7021, CNRS/Université de Strasbourg, 74 route du Rhin, 67401 Illkirch-Graffenstaden, France

KEYWORDS: Block copolymers, fluorescence labeling, encapsulation, drug delivery, FRET, ratiometric imaging.

ABSTRACT: Polymeric nanoparticles (NPs) continue to assert their high potential as efficient nanovectors for nanomedicine and imaging agents. Among them, biocompatible polyesters block copolymers (BCP) possess appealing features as their physicochemical properties can be readily modified by the composition of their blocks. Although the fluorescent labeling of polymers is often used to track the formed NPs in bioimaging, it is rarely used to characterize their physicochemical properties. In this work we assumed that the branching degree of the hydrophobic block copolymer might play an important role in the properties of the biocompatible NPs and thus could help in controlling their cargo encapsulation and release. To this end clickable PEG-PCL block copolymers with various branching degrees were synthesized. Owing to their covalent fluorescent labeling using strain-promoted azide-alkyne cycloaddition (SPAAC), several parameters like the critical aggregation concentration of the BCPs as well as the colloidal stability, the core polarity and stealth of the NPs have been studied. Taking advantage of the fluorescence labeling of the NPs' core, their ability to encapsulate and release a fluorescent cargo (Rhodamine C₁₈) was assessed by Förster Resonance Energy Transfer (FRET). The observed differences in release profile was confirmed in cells where the fluorescent NPs and their cargo were tracked. Finally, the cargo release of endocytosed NPs was imaged and assessed by FRET ratiometric imaging. This study proved that the covalent fluorescent labeling of the BCPs is an efficient tool, offering various methods to characterize and assess the effects of polymers modifications on the NPs' properties.

INTRODUCTION

New drug delivery materials are continuously asserting their importance for the development of innovative treatment strategies.¹ The use of nanovectors like nanoparticles (NPs) has revolutionized the administration of medicines,² by protecting them and thus improving their bioavailability, therapeutic efficacy, specificity but also by lowering their toxicity.^{3,4} Among these nanovectors, polymeric NPs stand out from others by their high loading capability, their accessible surface modification for targeting and their lowered cytotoxicity.⁵ The major advantage of polymeric NPs lies in the possibility to modulate their composition by chemical modifications, leading to new encapsulation and release properties.⁶ To control and modify these parameters, the polymer itself should present adjustable properties. Among organic polymers, block copolymers (BCPs) display appealing features as they are composed of two or more blocks, each with specific physicochemical properties or functionalities, offering opportunities of combination to develop new materials.^{7,8} BCPs are often composed of at least a hydrophobic and a hydrophilic blocks, leading to amphiphilic macromolecules, generally resulting in NPs presenting a core/shell structure.⁹ Advantageously, BCPs composed of PEG and polyesters like poly(lactic-co-glycolic acid) (PLGA), poly lactic acid (PLA) or polycaprolactone (PCL) are the most commonly used due to their respective biocompatibility and biodegradability.^{10–12} Consequently, nanomaterials arisen from these BCPs were widely studied as nanovectors for drug delivery.^{13,14} NPs composed of PEG-PCL have drawn a specific interest as promising vectors for nanomedicines.¹⁵ In order to study the structure/drug delivery relationship of these PEG-PCL-based NPs, several parameters have already been varied including: the length of hydrophobic/hydrophilic blocks,¹⁶ the ratio between hydrophobic/hydrophilic blocks,¹⁷ the number of various blocks per chain,¹⁸ the combination and the ratio between diblock and triblock chains¹⁹ or the nature

and the functionalization of blocks.^{20, 21} Additionally, the shape of the polymeric structure (linear, 3, or 4-arms, brush and branched) can also be varied through the modification of initiator or the addition of branching agent.^{22–24} These modifications mainly alter the balance between the hydrophobic and hydrophilic blocks and can improve the solubility, the encapsulation or the release of the cargo.

In general, the influence of these parameters is assessed by time consuming HPLC analysis²⁵ or low sensitivity UV-visible spectroscopy.²⁶ Moreover, these methods only report on the drug loading and the amount of drug released, providing no information about the physicochemical properties of the NPs and their behavior in a biological environment. The fluorescence is a powerful tool which is already used to image materials and to track them in biological environment.^{27,28} In this regard, we recently reviewed the different chemical approaches to fluorescently label block copolymers and their applications in bioimaging.²⁹ Although the fluorescent labeling is mainly used for bioimaging applications, it can also allow to understand the formation of NPs,³⁰ to characterize their properties,³¹ to sense cellular environments,³² and to assess the cargo encapsulation and monitor the release.^{33, 34} Consequently, the fluorescent labeling can help to determine the physicochemical properties of the BCPs and of the resulting NPs.

Herein, we studied the influence of the branching on PEG-PCL block copolymers obtained through the copolymerization of PEG, ϵ -caprolactone, azido-caprolactone³⁵ and glycidol³⁶ as branching agent. These polymeric chains were fluorescently labeled by click chemistry using BODIPY and the solvatochromic Nile Red. Thanks to this labeling, the aggregation, the colloidal stability, the stealth character and the core polarity of the resulting NPs were studied. Then, the encapsulation and the release of a fluorescent drug model were assessed and monitored using FRET in *in vitro* and *in cellulo* assays.

MATERIALS AND METHODS

Materials. PBS (phosphate buffer saline) pH 7.4 was purchased from Eurobio (Gourtaboeuf, France). FBS (fetal bovin serum) was purchased from Lonza. Rhodamine-C₁₈ perchlorate was purchased from ABCR GmbH.

Synthesis. All starting materials for synthesis were purchased from Alfa Aesar, Sigma-Aldrich or TCI Europe and used as received unless stated otherwise. PEG2000 was purchased from Clariant. Caprolactone and N₃-caprolactone were purchased from Alfa Aesar. NMR spectra were recorded on a Bruker Avance III 400 MHz spectrometer. Mass spectra were recorded using an Agilent Q-TOF 6520 mass spectrometer. Protocols for synthesis and characterizations of all new compounds including polymers, NR-DBCO, BDP-DBCO, and Rhod-C₁₈ are given in the supporting information (SI).

Polymerization. To a solution of PEG (0.25 mmol, 1 eq), ϵ -caprolactone (10.92 mmol, 43.7 eq), N₃-caprolactone (0.32 mmol, 1.3 eq) and glycidol (0, 1, 3 or 7 eq) were dissolved in 1,2-dichloroethane under inert atmosphere (Argon). The mixture was heated at 100 °C for 3 h using a Dean-Stark apparatus to remove traces of water. Then, a drop of Tin(II) 2-ethylhexanoate (Sn(Oct)₂) was added and the reaction was heated up at 120 °C. The reaction was allowed to stir for 16 h and the disappearance of the caprolactone monomers was monitored by TLC using DCM/MeOH, 9/1 as eluent. The solvent was evaporated and the resulting copolymer was dissolved in acetone and was precipitated in EtOH (1/4, acetone/EtOH).

Fluorescent labeling of polymer. PEG-PCL copolymer (50 mg), and BDP-DBCO or NR-DBCO (0.0034 mmol, 4.5 eq) were dissolved in DCM (3 mL), and the reaction mixture was allowed to stir at RT for 2 h. The solvents were evaporated and the crude was purified by size exclusion column using DCM/MeOH, 1/1. The yield of the reaction was calculated by measuring the absorbance of a 10 mg.mL⁻¹ solution of copolymer.

Formulation of NPs. 50 μ L of a copolymer solution (2.5 mg.mL⁻¹ in dioxane) was added to an Eppendorf tube and 950 μ L of PBS was vigorously added by back and forth pipetting using a 1 mL micropipette. The solution was immediately vortexed for 10 seconds. For the fluorescently labeled NPs, solutions of non-labeled polymer and fluorescently labeled polymer (2.5 mg.mL⁻¹ in dioxane) were mixed so that the concentration of BODIPY was set to 30 μ M. After formulation (20-fold dilution), the final concentrations were 125 μ g.mL⁻¹ of copolymers and 1.5 μ M of BODIPY.

Encapsulation of acceptors. 50 μ L of dioxane solution containing a mixture of labeled and non-labeled copolymers (2.5 mg.mL⁻¹, BODIPY concentration 30 μ M) and the acceptor rhodamine (0 to 12 μ M) was added to an Eppendorf tube and 950 μ L of PBS was vigorously added by back and forth pipetting using a 1 mL micropipette. After formulation, the final concentrations were 125 μ g.mL⁻¹ of copolymers, 1.5 μ M of BODIPY and 0 to 0.6 μ M of rhodamine.

Determination of CAC using free Nile Red. 50 μ L of dioxane solution with an increasing concentration of copolymers and a fixed concentration of Nile Red (0.2 μ M) was added to an Eppendorf tube. Then, the NPs were formulated as

described above. For each copolymer, a gradient of copolymers concentrations was performed from 0.1 to 16 μ M.

Determination of CAC using Nile Red-labeled BCPS. 50 μ L of dioxane solution with an increasing concentration of copolymer (95% of non-labeled copolymer and 5% of NR-labeled copolymer) was added to an Eppendorf tube. Then, the NPs were formulated as described above. For each copolymer, a gradient of copolymers concentrations was performed from 0.05 to 16 μ M.

Reduction of the interfacial NR. Nile Red-labeled NPs (containing 5% Nile Red-labeled BCPS) were formulated according to the protocol described above. 500 μ L of the solution was diluted with PBS and the other 500 μ L by PBS containing sodium dithionite (40 mM). The emission spectra were recorded right after dilution.

Dynamic light scattering. The sizes of NPs were measured by dynamic light scattering using the instrument Zetasizer® Nano ZSP (Malvern, UK). Measurements were performed at 25 °C. Both size distribution and the dispersity (\mathcal{D}) were recorded.

Gel permeation chromatography (GPC). To a solution of copolymers in anhydrous THF (10 mg.mL⁻¹), two drops of a solution containing 10 v/v % of toluene in THF was added. Then, the solution was filtered (0.45 μ m, PTFE). The samples were measured by GPC-Refractive Index (JASCO-RI 4030 with Shodex-GPC-KF805L column) using THF as eluent and conventional calibration with polystyrene standards (from 1,650,000 to 580 g.mol⁻¹). The data were analyzed with the software ChromNAV.

Differential calorimetry scanning (DSC). 5-10 mg of copolymers were weighted in an aluminum crucible and analyzed by DSC (Q200, TA instrument). The calorimeter was calibrated from -80 °C to 300 °C. The data were analyzed with TA Universal Analysis software. The melting temperature (T_m) were determined on the second heating ramp. The degree of crystallinity (χ_c) was calculated for PEG-PCL samples using the following equation (Eq.1):

$$\chi_c = \frac{\Delta H_s}{\Delta H_{polymer}^{\circ}} \times 100 \quad (1)$$

Where ΔH_s is the released heat of the sample (J.g⁻¹) and ΔH° is the released heat of the same copolymer which is 100% crystallin. $\Delta H_{PCL}^{\circ} = 136 \text{ J.g}^{-1}$.

Samples were characterized with the following method: (1) heating ramp from 25 °C to 100 °C at 10 °C/min then isotherm for 3 min; (2) cooling ramp from 100 °C to -80 °C at 10 °C/min then isotherm for 3 min; (3) heating ramp from -80 °C to 100 °C at 10 °C/min then isotherm for 3 min and (4) cooling ramp from 100 °C to 25 °C at 10 °C/min.

Spectroscopy. Absorption and emission spectra were recorded on a Cary 5000 Scan ultraviolet-visible spectrophotometer (Varian) and a FS5 (Edinburgh Instruments) spectrofluorometer respectively. For standard recording of fluorescence spectra, the emission was collected 10 nm after the excitation wavelength. All the spectra were corrected from a wavelength-dependent response of the detector. Nile Red was excited at 500 nm and the spectra were recorded from 510 to 800 nm. BODIPY was excited at 460 nm and the spectra were recorded from 470 to 700 nm. The extinction molar coefficient (ϵ) used for titration were 80,000 M⁻¹.cm⁻¹ for the BODIPY and 38,000 M⁻¹.cm⁻¹ for the Nile Red (both in dioxane). The solvents were of spectroscopic grade. The quan-

tum yields, QY were determined by comparison with the reference following the equation (Eq.2):

$$QY = QY_R \times \frac{I \times OD_R \times n^2}{I_R \times OD \times n_R^2} \quad (2)$$

where I is the integrated fluorescence intensity, n is the refractive index, and OD is the optical density at the excitation wavelength. R represents the reference. For the BODIPY labeled BCPs, BODIPY 496/503 in water was used as reference.³⁷ FRET parameters were determined following the equations (Eq. 3 and 4):

$$\text{FRET ratio} = \frac{I_{\text{max}}(A)}{I_{\text{max}}(A) + I_{\text{max}}(D)} \times 100 \quad (3)$$

where $I_{\text{max}}(A)$ is the fluorescence intensity of the acceptor in FRET spectrum and $I_{\text{max}}(D)$ is the fluorescence intensity of the donor in FRET spectrum.

$$\text{FRET efficiency} = \left(1 - \frac{I_{\text{max}}(D)}{I_{\text{max}}(D_0)}\right) \times 100 \quad (4)$$

where $I_{\text{max}}(D)$ is the fluorescence intensity of the donor in FRET spectrum and $I_{\text{max}}(D_0)$ is the fluorescence intensity of donor in the absence of acceptor.

Kinetic of release. NPs were formulated as described above. 500 μL of the solution was diluted in PBS and the other 500 μL by 20 v/v % FBS in PBS. Emission spectra of the solution containing FBS were measured over 5 h. The measures were performed in triplicates.

Electrophoresis. Agarose gel (0.5 wt.%) was prepared in TAE (Tris Acetate 40 mM, EDTA 1 mM). 13 μL of the formulation solutions were carefully added in the wells. The electrophoresis was run at 125 V for 1 h. The gels were visualized with an ImageQuant LAS 4000 system (GE Healthcare Life science). Excitation was 473 nm and the fluorescent signal was collected using a 510 ± 10 nm filter with an exposition time of 10 seconds. The images were processed using ImageJ software.

Cellular imaging. KB cells (ATCC CCL-17) were grown in minimum essential medium (MEM, Gibco-Invitrogen) with 10 % fetal bovine serum (FBS, Lonza), 1 % non-essential amino acids (Gibco-Invitrogen), 1 % MEM vitamin solution (Gibco Invitrogen), 1 % L-glutamine (Sigma-Aldrich), and 0.1 % antibiotic solution (gentamicin, Sigma-Aldrich) at 37 °C in a humidified atmosphere containing 5 % CO_2 . For the imaging experiments, cells were seeded onto a 35 mm IBiDi live cell plates at a density of 1×10^5 cells/well 24 h before the microscopy measurement. Prior to incubation, NPs were formulated in Opti-MEM and their size were checked by DLS and showed similar sizes than in PBS (Table S2). Rhodamine- C_{18} loaded-NPs were then formulated in sterile Opti-MEM following the protocol described above and the solution was diluted 5 times to provide a NP solution with a copolymer concentration of 25 $\mu\text{g}\cdot\text{mL}^{-1}$. This solution was added to the cells, which were thereafter incubated at 37°C for 3 h in the presence of Hoechst (5 $\mu\text{g}\cdot\text{mL}^{-1}$) to stain the nuclei. The medium was then removed, washed 2 times with PBS and then fixed with 4% PFA for 10 min at room temperature. The medium was removed and the cells were washed with PBS and imaged in PBS. The fluorescence microscopy was performed on a Leica TSC SPE laser scanning confocal microscope with a 63X objective. The setting of the channels used were as follows: Donor (BODIPY): excitation laser 488 nm, fluorescence signal: 500-550 nm (green channel); Acceptor (Rhodamine): excitation laser 560 nm, fluorescence signal: 570-700 nm (green channel); FRET channel: excitation laser 488 nm, fluorescence

signal: 570-700 nm. The images are maximum intensity projections obtained from z-stacks with steps of 1 μm (minimum 6 images). The ratiometric images were obtained from the donor channel and the FRET channel using an ImageJ macro: "Ratio Intensity color 3.4" developed by Romain Vauchelles.

RESULTS AND DISCUSSION

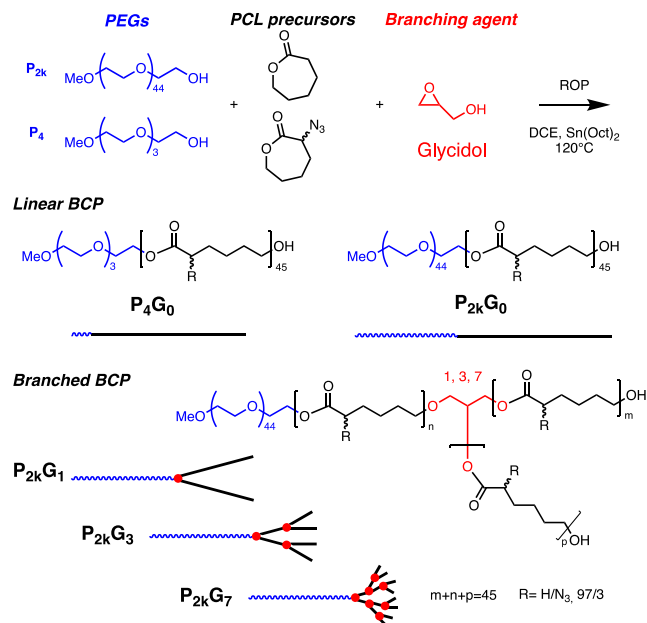


Figure 1. Synthesis of the clickable BCPs with increasing branching of the PCL block due to insertion of glycidol branching agent. For clarity, the schemes of the polymers do not represent their random distribution.

Design and synthesis. In order to study the effect of branching on polymeric NPs, we synthesized PEG-PCL amphiphilic polymers with PEG as hydrophilic block and PCL as hydrophobic one. PEG2000 was chosen to provide sufficient hydrophilicity to the polymer and stealth to the NPs, which will avoid non-specific interactions and will ensure their colloidal stability in PBS. Then, the PEG/PCL ratio was fixed. We chose to synthesize block copolymers possessing an equimolar amount of ethylene glycol and caprolactone units. The block copolymers were thus synthesized by ring opening polymerization (ROP) using MeO-PEG-OH (PEG2000, MW 2000 Da) as initiator, which corresponds to 45 ethylene glycol units, and thus 45 equivalents of caprolactone. In order to incorporate a clickable site to the PCL block, an azido caprolactone (N₃-CL) was introduced in the ROP, corresponding to 3% of the total CL (Figure 1). Statistically, this proportion ensures at least one azide function per copolymer chain. Increasing amount of glycidol, *i.e.* 0, 1, 3, 7 eq (based on PEG) was added to the ROP to obtain PEG-PCL copolymers with increasing numbers of branching sites in the hydrophobic block, as showed in previous works.³⁶ This procedure gave rise to a linear BCP: P_{2k}G₀ and branched BCPs: P_{2k}G₁, P_{2k}G₃, and P_{2k}G₇ (Figure 1). Additionally, a linear copolymer possessing a small PEG (4 units), P₄G₀, was synthesized to study the influence of the PEG chain.

Characterizations. After purification by precipitation, the obtained copolymers were characterized by NMR. ^1H NMR showed that the copolymers were obtained in a pure form and confirmed the targeted PEG/PCL units ratios by integration of the methoxy group of the PEG (3.6 ppm) and the most shielded methylene group (CH_2O) of PCL unit (4.1 ppm) (**Figure 2A**, table). To prove the increasing insertion of glycidol in the copolymers, trichloroacetyl isocyanate was added to the NMR sample. Trichloroacetyl isocyanate spontaneously reacts with free hydroxyl groups and provokes an important shift (3.6 to 4.2 ppm) of the methylene groups (CH_2) that bears hydroxyl group due to the deshielding effect of the electron deficient trichloroacetyl carbamate group (Figure 2B).³⁸ Integration of this new shifted signal clearly showed an increasing amount of free hydroxyl groups upon branching thus suggesting the controlled insertion of glycidol units in the block copolymers (Figure 2B, Figure S1). Additionally, ^{13}C NMR study was performed to discriminate CL units involved in linear chains from those positioned at the terminal end of the polymer. This experiment showed that upon increase of branching, new CH_2 peaks appeared corresponding to the terminal CL units bearing a free hydroxyl group (Figure 2C, Figure S2).

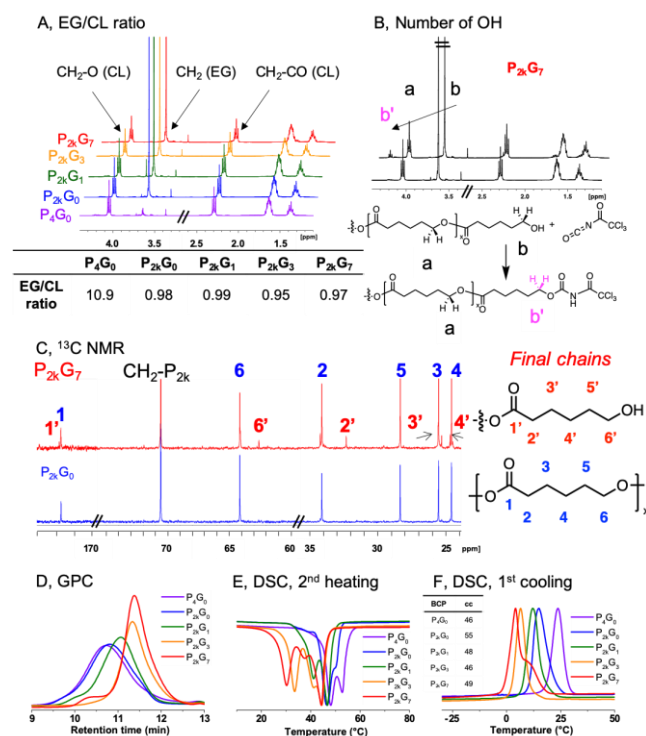


Figure 2. Characterization of the BCPs. (A) ^1H NMR spectra (400 MHz, CDCl_3) confirming the targeted EG/CL ratio indicated in table. (B) ^1H NMR spectra (400 MHz, CDCl_3) of P_{2k}G_7 and P_{2k}G_7 with trichloroacetyl isocyanate revealing the increasing number of free hydroxyl groups upon branching. (C) ^{13}C NMR spectra (126 MHz, CDCl_3) of P_{2k}G_0 and P_{2k}G_7 showing the apparition of shifted peaks upon branching. (D) GPC chromatograms (THF) depicting the increasing retention time and sharpness of the peak upon branching. (E) DSC second heating and (F) first cooling curves.

The copolymers were then submitted to gel permeation chromatography (GPC). Overall the results showed a general trend

where branching led to longer retention times along with sharper peaks (Figure 2D). This effect might be rather assigned to difference of conformations and steric effects due to the branching rather than the slight increase of molecular weight induced by the addition of small glycidol units (maximum +500 Da). Indeed, P_4G_0 and P_{2k}G_0 which have a difference of molecular weight of ~ 1800 Da, displayed overlaid GPC spectra. Although questioned in the literature for its limitations,³⁹ this GPC study showed a trend suggesting the effective difference of branching.

Finally, the copolymers were studied by differential scanning calorimetry (DSC). The results indicated that branching led to a decrease of fusion temperatures probably due to shorter PCL chain length (Figure 2E), along with lower crystallization temperatures due to insertion of structural amorphous defects within the copolymer chain (Figure 2F). These results are in line with previous report on branched PCL.³⁶ Overall these characterizations confirmed that PEG-PCL BCPs with increasing branching sites and different physicochemical properties have been obtained.

Fluorescence Labeling. Once the block copolymers fully characterized, the covalent fluorescent labeling has been achieved by strain-promoted azide-alkyne cycloaddition (SPAAC) that proved its efficiency in labeling block copolymers.²⁹ For this endeavor, two fluorophores were used. First, a bright green emitting BODIPY was used and served to study the stability and the stealth character of the NPs, and as a FRET donor to study the cargo encapsulation and cargo release (*vide infra*). The second is a Nile Red derivative,⁴⁰ which is highly solvatochromic and that will serve to determine the critical aggregation concentration (CAC) of the copolymers, as well as to evaluate their surface reactivity and the core polarity of the NPs. Both fluorophores, bearing a carboxylic acid function, were coupled to a DBCO- NH_2 unit to provide BODIPY-DBCO and NR-DBCO (**Figure 3**). The latter were clicked to the azide groups of the copolymers by SPAAC in mild conditions (Figure 3). The labeled copolymers were purified by size exclusion chromatography to remove any traces of free fluorophores. The efficiency of the labeling was assessed by absorbance spectroscopy providing yields ranging from 30 to 68% of labeled chains. NMR analysis confirmed that the polymers were not affected by the click conditions (Figure S3). Moreover, the success of this labeling reaction proved, *a posteriori*, the efficient insertion of N_3 -CL during the polymerization step (Figure 1).

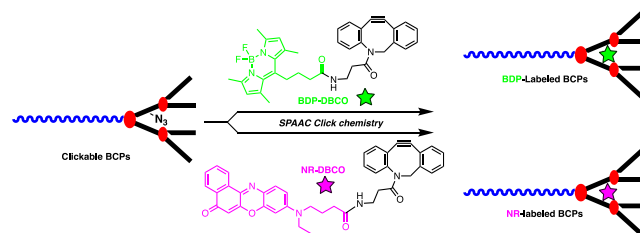


Figure 3. Fluorescent labeling of the BCPs by a green emitting BODIPY fluorophore and an environment sensitive Nile Red probe, using SPAAC click chemistry. The solvent was DCM. All the BCPs were labeled, P_{2k}G_3 was given as an example.

Formulation. Prior to the formulation of the NPs, the critical aggregation concentration (CAC) of the copolymers were measured to evaluate the concentration at which the copoly-

mer could form NPs. Nile Red is a valuable fluorescent tool to evaluate CMC of surfactant or CAC of polymer by spectroscopy.^{41,42} Indeed, Nile Red fluorescence intensity and λ_{max} (Em) respectively increases and blue shifts when the hydrophobic core of micelles or NPs are formed. In a first attempt, the non-labeled copolymers were formulated in PBS at various concentrations in the presence of a fixed concentration of Nile Red (Figure 4A top). Surprisingly, the CAC were found to be similar for each polymer (~1-2 μM), even for the highly hydrophobic P_4G_0 (Figure 4B top). These results suggested that at this concentration Nile Red was not able to report submicromolar CAC as its affinity towards the precipitated

polymer is probably insufficient, so that it remained mainly in the aqueous phase at low polymer concentration. To prove it, we took advantage of our NR-labeling BCPs, where Nile Red moiety acts as an internal reporter (Figure 4A, bottom). Solutions of copolymers containing 5% of their NR-labeled cognates were diluted in PBS at various concentrations. The results showed that the NR reporter displayed a constant blue shifted emission maximum (around 634 nm) compared to free NR in water (660 nm), even at low concentrations (Figure 4B bottom). These results suggested that the CACs were below 50 nM (~350 ng/mL) and confirmed the relatively high hydrophobic nature of the copolymers.

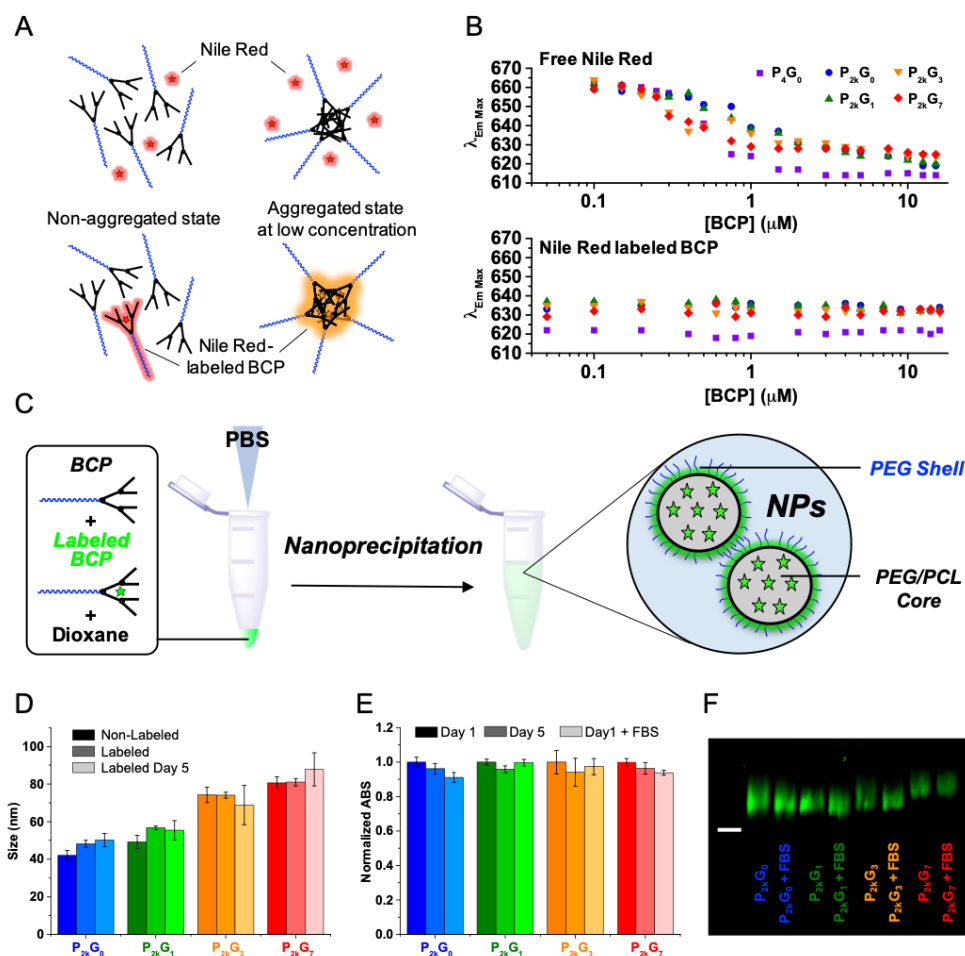


Figure 4. Formulation and stability of the NPs. (A) Determination of the critical aggregation concentration using free NR (top) or NR-labeled BCPs (bottom). (B) plot of NR λ_{max} (Em) upon increase of the BCPs concentration using free NR (top) or NR-labeled BCPs (bottom). (C) Formulation of the polymeric NPs by nanoprecipitation. (D) Size of the non-labeled and labeled NPs and assessment of their colloidal stability after 5 days. (E) Relative absorbance of labeled NPs (values were normalized to 1 for NPs at day 1), right after formulation, after 5 days and in the presence of 10 v/v % FBS. (F) Electrophoresis of the labeled NPs and NPs in the presence of 10 v/v % FBS showing their stealth. Scale bar is 5 mm and indicate the level of the wells.

Subsequently, the NPs were formulated in PBS by nanoprecipitation, way above the CAC, at a final copolymer concentration of 125 $\mu\text{g}\cdot\text{mL}^{-1}$ (Figure 4C). To obtain fluorescent NPs, the non-labeled copolymer were mixed with a small amount of BDP-labeled BCP (~6 wt.%) to avoid aggregation caused quenching of the fluorophores and thus ensuring a high quantum yield.⁴³ The sizes of the obtained NPs were measured by dynamic light scattering (DLS). Except for P_4G_0 which formed polydisperse large size NPs due to its small PEG chain (data not shown), NPs were obtained with sizes ranging from

42 \pm 3 nm to 81 \pm 3 nm (Figure 4D) with good polydispersity indexes (from 0.10 to 0.18). Interestingly, the results clearly indicated that branching of the PCL block led to larger NPs (Figure 4D). In addition, formulation in the presence of fluorescently labeled-BCPs did not significantly change the obtained sizes (Figure 4D), suggesting that fluorescent labeling did not affect the nanoprecipitation of the polymer. The colloidal stability of the NPs was assessed by measuring their sizes over the time. After 5 days the mean size did not display

a significant change, however an increase of the polydispersity index was observed (from 0.22 to 0.48).

Taking advantage of the BODIPY labeling, absorption spectra of the labeled NPs were measured over the time, which revealed that only 4% of the signal was lost over 5 days, thus depicting a good colloidal stability over this period (Figure 4E). Further measurements after several weeks indicated that the NPs gradually lose their colloidal stability, which conduct us to freshly formulate the NPs prior to any studies. To study the stealth properties of the NPs, the latter were put in the presence of 10 v/v % Fetal Bovine Serum (FBS) that is composed of various amphiphilic biomolecules that could interact with the NPs.^{44, 45} The absorption spectra were only slightly affected by the presence of FBS (Figure 4E), identical observations were made with fluorescence spectra (Figure S4). To better assess their stealth character, the NPs were analyzed by electrophoresis in absence and presence of FBS. The image revealed that the NPs due to their non-charged nature, only slightly move towards the anode (Figure 4F). Moreover, their migration was poorly affected by 10 v/v % FBS suggesting that the NPs did not interact with biomolecules from FBS, thus showing a high stealth degree. Overall, despite the low CAC values due to relatively high hydrophobic nature of the copolymers, the formulated NPs were found to be rather stable over the time and presented a strong stealth character, which are desirable features of nanocarriers used for drug delivery.

Determination of NPs core polarity. As discussed earlier, branching of the BCP provoked the shortening of the PCL chains along with their increasing number and thus of the terminal hydroxyl groups (Figure 2B and C). Consequently, we assumed that the branching of BCP could have an effect on the polarity of the polymeric matrix which in return could directly influence the cargo encapsulation efficiency as well as the cargo release. To evaluate the polarity of the polymeric matrix of the NPs, we formulated NPs composed of 5% Nile Red-labeled BCP (Figure 5A).

Nile Red, as an electron deficient dye is readily reduced by sodium dithionite. This property has been successfully used to evaluate the flip flop of membrane probes at the surface of lipid vesicles, and to selectively remove NR signal at the cell plasma membrane,⁴⁶ by selective bleaching of the interfacial and water-exposed NR. Herein, we used this property to assess the dye repartition within the NPs and to probe the polarity of the NPs' core. Indeed, Nile Red that is exposed at the NP/water interface is quickly reduced by water soluble dithionite whereas deeply embedded NR is protected from the reduction (Figure 5A). Upon addition of dithionite the fluorescence signal is thus decreased, which was accompanied with a hypsochromic shift due to the preserved NR embedded in the more hydrophobic core (Figure 5B). Consequently, sodium dithionite was added to solutions of NR-labeled NPs and the fluorescence loss was measured. The results showed a clear trend where NPs arising from branched copolymers were more resistant to the dithionite reduction (Figure 5C). This observation might be assigned to the difference in the NPs size. Indeed, larger particles have lower surface/volume ratio thus providing lower amount of accessible dyes at the NP/water interface.

Interestingly, prior to addition of sodium dithionite, the NR-labeled NPs displayed similar maximum emission wavelength (~632 nm, figure 5C). After “bleaching” of the interfacial NR,

this value significantly decreased to reach different values depending on the branching of the BCPs (Figure 5C). The difference in the emission wavelength (before and after reduction) gradually decreased from 18 nm to 5 nm from the less branched $P_{2k}G_0$ to the more branched $P_{2k}G_7$. This experiment confirmed that NPs with branched copolymers possess more polar cores. These observations were confirmed with the most hydrophobic P_4G_0 where the loss of fluorescence intensity was only 22% with a negligible shift of λ_{max} (Em) (1 nm). Overall these observed differences of polarity might influence the cargo encapsulation and release ability of the NPs.

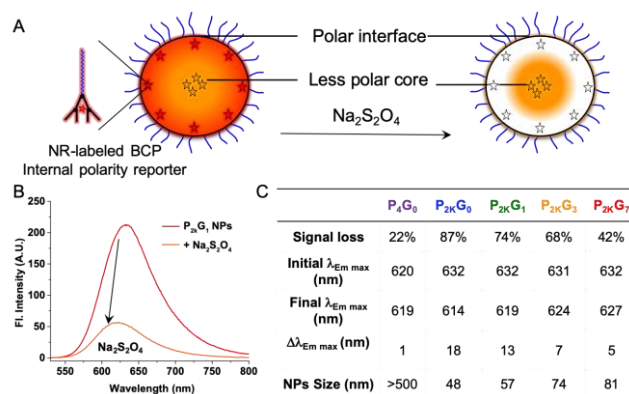


Figure 5. Determination of the core polarity of NPs using NR-labeled BCP as reporter. (A) NR-labeled NPs were formulated and sodium dithionite bleached the interfacial NR reporter. (B) As an example, emission spectra of $P_{2k}G_1$ before and after addition of sodium dithionite depicting the signal loss and the hypsochromic shift due to the interfacial bleaching of NR. (C) Data obtained from the interfacial bleaching experiment of the different NPs, the size of the NPs were added as a reminder. Excitation wavelength was 500 nm.

Encapsulation and release assessed by FRET. In order to study the influence of the BCP branching on encapsulation and release of cargo molecules, FRET experiments were designed with an efficient FRET couple,^{47,48} where the green fluorescent polymer matrix was used as a FRET donor and red emitting rhodamines as FRET acceptor and model cargo (Figure 6). To this end, a hydrophobic rhodamine bearing a stearic ester (C_{18} chain) was used. To assess the effect of the cargo polarity on the encapsulation and release, the perchlorate ion was replaced by bulky hydrophobic anions tetraphenylborate (TPB) and perfluorinated tetraphenylborate (F_5 -TPB) (Figure 6A, details in SI), which were shown to improve encapsulation cationic dyes and prevent their self-quenching.^{49, 50} The cargo rhodamines were dissolved in dioxane with the copolymers and were encapsulated by nanoprecipitation (Figure 6B). The spectral study of the obtained particles allowed to study the encapsulation efficiency by measuring the FRET ratio and FRET efficiency whereas the FRET decrease allowed to assess the release of the acceptor cargo in the presence of fetal bovine serum (FBS) (Figure 6C).

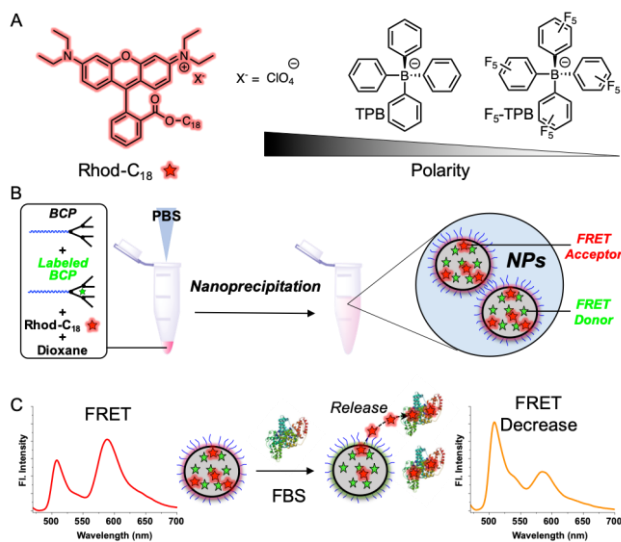


Figure 6. Encapsulation and release of rhodamines. (A) Rhodamine- C_{18} with counterions displaying a decreasing polarity used for encapsulation in NPs. (B) Encapsulation of the Rhodamine acceptors by nanoprecipitation leading to FRET NPs. (C) Release of the rhodamine acceptor in the presence of FBS leading to a FRET decrease.

Prior to the encapsulation and release spectroscopic studies, the quantum yields of the BDP-labeled NPs were evaluated to ensure the ability of these nanocarriers to transfer sufficient energy. After formulation in PBS the BDP-labeled NPs displayed high quantum yields ranging from 0.68 to 0.82 (See table S1). BDP-labeled NPs with different branched matrix were then formulated with the different rhodamines at a fixed donor (BDP)/acceptor (Rhod) ratio of 2.5. Thereafter, the emission spectra were recorded (Figure 7A-C) and analyzed to assess the FRET ratio and FRET efficiency (Figure 7D-F). In all cases, FRET occurred with a relatively high efficiency (at least 57%) as the intensity of the donor clearly decreased upon encapsulation depicting the energy transfer phenomenon (Figure S5). The FRET efficiency clearly increased from Rhod- C_{18} - ClO_4 to the less polar rhodamines: Rhod- C_{18} -TPB and Rhod- C_{18} - F_5 -TPB thus suggesting a better encapsulation of the latter in the core of the NPs (Figure 7D and 7E-F respectively). Interestingly, the FRET ratio, which also informs about the restitution of the transferred energy into the acceptor fluorescence, significantly increased with the hydrophobicity of the rhodamine cargo (Rhod- C_{18} - ClO_4 < Rhod- C_{18} -TPB < Rhod- C_{18} - F_5 -TPB, Figure 7D-F). This effect is the most obvious with the linear $P_{2k}G_0$, where the FRET ratio increased upon increased hydrophobicity of the cargo rhodamine from 0.45 to 0.58 to 0.67.

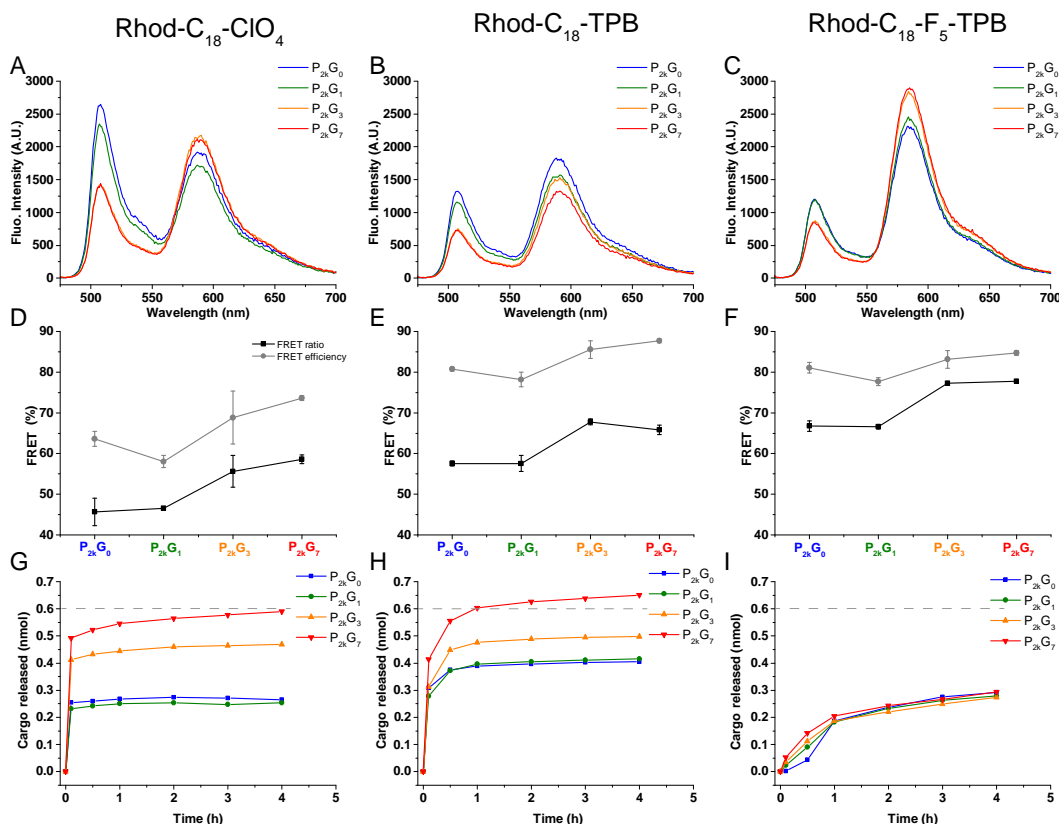


Figure 7. Encapsulation and release efficiency assessed by FRET. (A-C) Emission spectra of differently branched BCP based NPs encapsulating the three different Rhod- C_{18} cargos. (D-F) FRET ratio and FRET efficiency for the various formulations. (G-I) Release of the Rhod- C_{18} cargo in the presence of FBS (10 v/v %) assessed by the increase of the FRET acceptor/donor ratio. The dashed grey line indicates the maximum cargo release, corresponding to 0.6 nmol.

Overall these results revealed the encapsulation pattern of the cargo within the NPs. Indeed, the most polar rhodamine: Rhod-C₁₈-ClO₄ might accumulate at the NPs interface after their formation thus limiting the energy transfer to the interfacial surface. Conversely, the most hydrophobic rhodamines might precipitate with similar kinetics as the BCPs upon nanoprecipitation. Consequently, the FRET efficiency is higher with those hydrophobic cargos. However, upon formulation, Rhod-C₁₈-TPB can undergo significant self-quenching, in contrast to Rhod-C₁₈-F₅-TPB, where bulky fluorinated counterion prevents self-quenching of rhodamine dyes in the polymer matrix.^{49, 50} Therefore, FRET ratio values for Rhod-C₁₈-TPB were significantly lower compared to those of Rhod-C₁₈-F₅-TPB, despite their similar FRET efficiency (Figure 7E and F). Overall, these results are consistent with previous studies based on non-FRET polymeric NPs, showing that more hydrophobic counterions provide more efficient encapsulation of rhodamines into a polymer matrix.⁵⁰

Then, the results showed that branched copolymer-based NPs displayed higher FRET ratios within the same rhodamine series. For Rhod-C₁₈-ClO₄, where FRET is expected to mainly occur at the interface (*vide supra*), this trend not assigned to the difference in the NPs size. Indeed, large particles obtained with branched polymers have lower surface/volume ratio and would thus lead to lower FRET ratios. Consequently, these results suggested that branching enhanced the encapsulation and led to a more homogeneous repartition of the cargo within the polymer matrix.

Taking advantage of this FRET system, the release of the cargo can be directly assessed and quantified by the ratiometric readout of the FRET. For this endeavor, calibration curves were obtained by plotting the FRET acceptor/donor ratios against the quantity of the encapsulated rhodamine cargo (Figure S6). Then, to assess release of the cargo, FBS was added to the FRET NPs (loaded with 0.6 nmol of cargo), and the fluorescence emission spectra were measured at different time points. The calculation of FRET acceptor/donor ratios allowed us to obtain the released amount of rhodamine cargos (Figure 7 G-I). The analysis of the obtained release curves revealed valuable information. First of all, one can notice a clear-cut difference between the most polar cargos, *i.e.* Rhod-C₁₈-ClO₄ and Rhod-C₁₈-TPB in one hand and the most hydrophobic Rhod-C₁₈-F₅-TPB in the other hand. NPs incubated with the latter have identical slow release profiles regardless of the branching degree of the BCPs (Fig. 7I), all plateauing at 0.3 nmol (half of the maximum release). Conversely, the release profiles of NPs loaded with more polar Rhod-C₁₈-ClO₄ and Rhod-C₁₈-TPB showed an important influence of the BCP branching (Figure 7. G-H). Although the release of Rhod-C₁₈-ClO₄ was slightly faster than for Rhod-C₁₈-TPB, their release profiles were quite similar. Interestingly, despite their large size (82 nm), NPs-based on the highly branched BCP P_{2k}G₇ quickly released the totality of its cargo (0.6 nmol) whereas the other NPs did not reach the maximum amount of released cargo suggesting that less branched BCP allow to keep a reservoir of cargo within the core of the NPs. In addition, figure 7G-H showed a trend proving that gradual increasing of BCP branching can help in controlling the portion of burst release and the reservoir of the cargo. The burst release is assigned to cargo located at the water interface of the NPs, whereas the reservoir cargo might be tightly encapsulated in the polymeric core matrix. Overall, these results sug-

gested that the branching of BCP enable the control of the cargo release depending on the nature of the latter.

Cellular Imaging. Finally, the effect of the branching of the copolymers on the interaction of NPs with cells was evaluated by laser scanning microscopy. At first, the cell permeability of the NPs was evaluated. After checking that the size of the NPs was not affected when formulated in the growing media (Table S2), BDP-labeled NPs were incubated with KB cells for 3 h, before being washed and fixed. As expected, the NPs displayed low cell permeability due to their high stealth character. Although NPs obtained from linear BCP P_{2k}G₀ and the lower branched BCP P_{2k}G₁ did not display any signal corresponding to the NPs, those obtained from branched copolymers P_{2k}G₃ and P_{2k}G₇ provided signs of cell penetration (Figure S7). This difference of cell penetration might be assigned to the difference of the polymer polarity or the various NPs size. A dedicated study would be necessary to conclude regarding this phenomenon. However, a dedicated study would be required to conclude about these differences. The punctiform distribution of the green fluorescence signal and their movement in live cells (Movie 1), indicated that these NPs penetrate through endocytosis. The NPs with the higher cell penetration ability, *i.e.* composed of P_{2k}G₇, were thus chosen to study the cargo release. Rhodamine-loaded P_{2k}G₇ NPs were incubated with cells and were fixed before being imaged. Recording the green and red signal allowed to independently monitor the fate of the NPs and the rhodamine cargo, respectively (Figure 8 A-C).

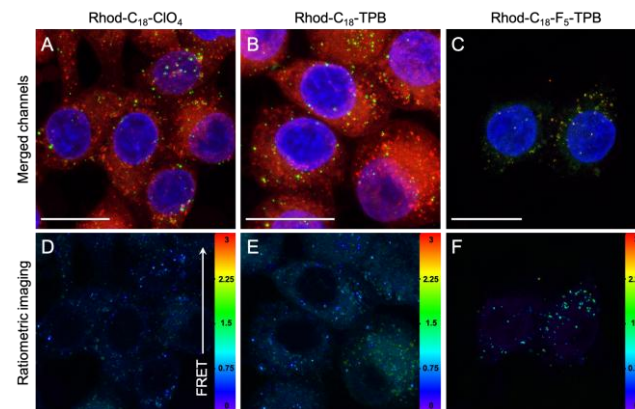


Figure 8. Laser scanning imaging of KB cells incubated with P_{2k}G₇ BCPs NPs encapsulating various cargos: Rhod-C₁₈ ClO₄ (A, B), Rhod-C₁₈ TPB (C, D) and Rhod-C₁₈ F₅-TPB (E, F). (A, B, C) The green and red channels indicate the location of the NPs and the cargo respectively. (D, E, F) FRET ratio imaging indicating the release of the cargo from the NPs. The nuclei were stained with Hoechst (5 µg.mL⁻¹), scale bar is 20 µm.

In the case of Rhod-C₁₈-ClO₄ and Rhod-C₁₈-TPB, the green punctiform signal is clearly separated from the red cytoplasmic signal with low colocalization, showing an important release of the cargo from the NPs. The rainbow color coded ratiometric imaging using the green channel and the FRET channel (excitation of the donor, emission from the acceptor) confirmed the high release of the cargo with spots corresponding to the endocytosed NPs displaying low FRET ratios (Figure 8D, E). Conversely, NPs encapsulating Rhod-C₁₈-F₅-TPB displayed spots with colocalized green and red signals (Figure 8C). It is important to note that the NPs that overlay the nucleus are actually above the latter as images in figure 8 arise from maximum intensity projections from a Z stack of several im-

ages (see Cellular imaging in the materials and methods section). The FRET ratio imaging clearly indicated that the cargo mainly remained in the NPs as the spots display FRET ratios of higher values (Figure 8F). Overall, the cell imaging confirmed the trend observed in *in vitro* release experiments assessed by FRET (Figure 7 G-I) and that Rhod-C₁₈ F₅-TPB remain tightly encapsulated in NPs even once the latter got internalized in cells. These results are in line with the previous studies showing that bulky counterions F₅-TPB due to its low polarity prevents dye leakage from polymeric NPs.⁵⁰ Further experiments conducted with Rhod-C₁₈ F₅-TPB loaded P_{2k}G₇-

based NPs demonstrated the interest of the ratiometric imaging. Unlike the merge of the green and FRET signal which only provided intensity-coded images (Figure 9A), the ratiometric imaging displayed color-coded images directly related to the FRET and informing on the release state of the NPs (Figure 9B). Interestingly, ratiometric images also indicated that a single cell possesses various populations of vesicles where the cargo is more or less released or encapsulated (Figure 9C). These results suggest that using advanced microscopy, the cargo release from NPs could be monitored at the level of a single vesicle in live cells.

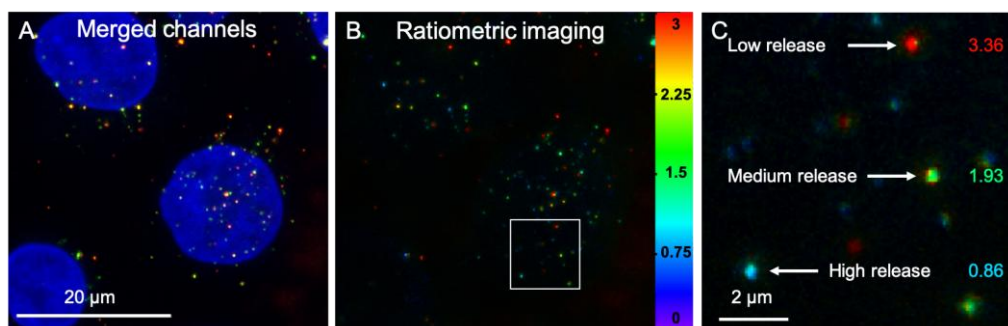


Figure 9. Laser scanning imaging of KB cells incubated with Rhod-C₁₈ F₅-TPB loaded P_{2k}G₇ BCP NPs. (A) Merge of the green and FRET signal. (B) ratiometric image obtained from the green and FRET channel. (C) Zoom of the region of interest in B, where vesicles of different ratio values are visible indicating difference of cargo release within the same cell. The nuclei were stained with Hoechst (5 μg.mL⁻¹), scale bar is 20 μm.

CONCLUSION

Block copolymers constitute a unique platform for the development of new materials with controlled properties. Indeed, slight modifications of their composition can lead to important change of their physicochemical properties that, in return, can influence the encapsulation and release of cargos for drug delivery applications. The branching degree of the non-polar block PCL was herein modified by introduction of branching agent (glycidol). The insertion of these branching points in the BCPs was characterized by ¹H and ¹³C NMR. Conventional techniques including GPC and DSC clearly indicated that those modifications significantly modified the physicochemical properties of the BCPs. Introduction of small amount of an azido-caprolactone monomer during the ring opening polymerization step allowed to obtain clickable BCPs. This feature was used to label the BCPs with fluorescent probes in mild conditions using SPAAC.

The labeling with a green emitting BODIPY, in a first part, helped to assess the colloidal stability and the stealth of the NPs. The labeling with the solvatochromic Nile Red allowed to determine the CAC of the BCPs (below 50 nM), whereas the use of free Nile Red resulted in misleading data. Additionally, the labeled-BCPs with Nile Red served to show that NPs arisen from branched BCPs possessed more polar cores. After characterizing the NPs with fluorescence techniques, the BDP-labeled BCPs were used to study the encapsulation and release of fluorescent rhodamine cargos providing a FRET ratiometric readout. The FRET efficiencies and ratios tended to show that branched BCPs enabled a better encapsu-

lation of the cargos along with a more efficient release depending on the polarity of the latter.

When incubated with cells, NPs obtained from branched BCPs were shown to penetrate more efficiently. When cell imaging of acceptors loaded P_{2k}G₇ NPs was performed, both NPs and cargo have been tracked individually and confirmed that non-polar cargo based on a cation dye and bulky hydrophobic counterions, Rhod-C₁₈-F₅-TPB, remained tightly encapsulated in their polymeric vectors.

Finally, further analysis of the ratiometric imaging allowed us to show that within a same cell, coexist vesicles containing NPs with different cargo release profiles, that can be assigned to different stages of their endocytic pathway. In conclusion, the fluorescent labeling of BCPs with fluorophores like BODIPY or fluorescent probe like Nile Red gave rise to various methods to characterize both polymers and NPs providing important information for the encapsulation and release of cargos using both spectroscopy and microscopy.

This approach led us to conclude that branching of the BCPs' hydrophobic block clearly affects their physicochemical properties as well as those of the formed NPs. We believe that the methods described herein could easily be applied in laboratories and will hopefully lead to the development of NPs for biomedical applications.

ASSOCIATED CONTENT

Supporting Information

Protocols of synthesis, characterization of new compounds including ¹H NMR and ¹³C NMR and high-resolution mass spectra, and supplementary figures including spectroscopic characterizations

and cell permeability studies of the NPs can be found in the supplementary information.

Movie 1. Time laps of live KB cells incubated with P_{2k}G₇ BCP NPs. The Supporting Information is available free of charge on the ACS Publications website.

AUTHOR INFORMATION

Corresponding Author

* mayeul.collot@unistra.fr

Funding Sources

This work was funded by MedinCell SA (France) and the French ministry of research (Ministère de l'enseignement supérieur, de la recherche et de l'innovation).

ACKNOWLEDGMENT

The authors would like to thank the Chemlab platform, (ECPM-Strasbourg) for the GPC and DSC analyses, Dr. Dmytro Danylchuk for providing Nile Red-COOH, Dr. Caterina Severi for providing Rhod-C₁₈-F₅-TPB and Dr. Delphine Garnier from the PACSI analysis platform for her help. A special thank is addressed to Romain Vauchelles for the development of the macro "Ratio Intensity color 3.4".

ABBREVIATIONS

PBS, Phosphate Buffer Saline; FBS, Fetal Bovin Serum; FRET, Förster Resonance Energy Transfer; TPB, TetraPhenylBorate; BCP, Block CoPolymer; GPC, Gel Permeation Chromatography; DSC, Differential Scanning Calorimetry; PEG, PolyEthyleneGlycol; PCL, PolyCaproLactone; ROP, Ring Opening Polymerization; NMR, Nuclear Magnetic Resonance; DBCO, DiBenzoCycloOctyne; NPs, NanoParticles;

REFERENCES

- (1) Tiwari, G.; Tiwari, R.; Sriwastawa, B.; Bhati, L.; Pandey, S.; Pandey, P.; Bannerjee, S. K. Drug Delivery Systems: An Updated Review. *Int. J. Pharm. Investig.* **2012**, *2* (1), 2–11. <https://doi.org/10.4103/2230-973X.96920>.
- (2) Couvreur, P. Nanoparticles in Drug Delivery: Past, Present and Future. *Adv. Drug Deliv. Rev.* **2013**, *65* (1), 21–23. <https://doi.org/10.1016/j.addr.2012.04.010>.
- (3) de Jong. Drug Delivery and Nanoparticles: Applications and Hazards. *Int. J. Nanomedicine* **2008**, 133. <https://doi.org/10.2147/IJN.S596>.
- (4) Lammers, T.; Kiessling, F.; Hennink, W. E.; Storm, G. Drug Targeting to Tumors: Principles, Pitfalls and (Pre-) Clinical Progress. *J. Controlled Release* **2012**, *161* (2), 175–187. <https://doi.org/10.1016/j.jconrel.2011.09.063>.
- (5) Yu, X.; Trase, I.; Ren, M.; Duval, K.; Guo, X.; Chen, Z. Design of Nanoparticle-Based Carriers for Targeted Drug Delivery. *J. Nanomater.* **2016**, *2016*, 1–15. <https://doi.org/10.1155/2016/1087250>.
- (6) Nicolas, J.; Mura, S.; Brambilla, D.; Mackiewicz, N.; Couvreur, P. Design, Functionalization Strategies and Biomedical Applications of Targeted Biodegradable/Biocompatible Polymer-Based Nanocarriers for Drug Delivery. *Chem Soc Rev* **2013**, *42* (3), 1147–1235. <https://doi.org/10.1039/C2CS35265F>.
- (7) Dawkins, J. Block Copolymers: Synthetic Strategies, Physical Properties and Applications. N Hadjichristidis, S Pispas and GA Floudas. John Wiley & Sons, Ltd, Chichester, UK, 2002. Pp 440, ISBN 0-471-39436-x. *Polym. Int.* **2004**, *53* (2), 232–232. <https://doi.org/10.1002/pi.1313>.
- (8) Becker, G.; Wurm, F. R. Functional Biodegradable Polymers via Ring-Opening Polymerization of Monomers without Protective Groups. *Chem. Soc. Rev.* **2018**, *47* (20), 7739–7782. <https://doi.org/10.1039/C8CS00531A>.
- (9) Robin, M. P.; O'Reilly, R. K. Strategies for Preparing Fluorescently Labelled Polymer Nanoparticles: Designing Fluorescent Polymer Nanoparticles. *Polym. Int.* **2015**, *64* (2), 174–182. <https://doi.org/10.1002/pi.4842>.
- (10) Kamaly, N.; Xiao, Z.; Valencia, P. M.; Radovic-Moreno, A. F.; Farokhzad, O. C. Targeted Polymeric Therapeutic Nanoparticles: Design, Development and Clinical Translation. *Chem. Soc. Rev.* **2012**, *41* (7), 2971. <https://doi.org/10.1039/c2cs15344k>.
- (11) Weiss, B.; Schaefer, U. F.; Zapp, J.; Lamprecht, A.; Stallmach, A.; Lehr, C.-M. Nanoparticles Made of Fluorescence-Labelled Poly(L-Lactide-Co-Glycolide): Preparation, Stability, and Biocompatibility. *J. Nanosci. Nanotechnol.* **2006**, *6* (9), 3048–3056. <https://doi.org/10.1166/jnn.2006.424>.
- (12) Sinha, V. R.; Bansal, K.; Kaushik, R.; Kumria, R.; Trehan, A. Poly-ε-Caprolactone Microspheres and Nanospheres: An Overview. *Int. J. Pharm.* **2004**, *278* (1), 1–23. <https://doi.org/10.1016/j.ijpharm.2004.01.044>.
- (13) Ashour, A. E.; Badran, M. M.; Kumar, A.; Rishi, A. K.; Yassin, A. E. Di-Block PLCL and Tri-Block PLCLG Matrix Polymeric Nanoparticles Enhanced the Anticancer Activity of Loaded 5-Fluorouracil. *IEEE Trans. NanoBioscience* **2016**, *15* (7), 739–747. <https://doi.org/10.1109/TNB.2016.2612340>.
- (14) Zhang, Y.; Luo, S.; Liang, Y.; Zhang, H.; Peng, X.; He, B.; Li, S. Synthesis, Characterization, and Property of Biodegradable PEG-PCL-PLA Terpolymers with Miktoarm Star and Triblock Architectures as Drug Carriers. *J. Biomater. Appl.* **2018**, *32* (8), 1139–1152. <https://doi.org/10.1177/0885328217751247>.
- (15) Grossen, P.; Witzigmann, D.; Sieber, S.; Huwyler, J. PEG-PCL-Based Nanomedicines: A Biodegradable Drug Delivery System and Its Application. *J. Controlled Release* **2017**, *260*, 46–60. <https://doi.org/10.1016/j.jconrel.2017.05.028>.
- (16) Al Samad, A.; Bethry, A.; Koziolová, E.; Netopilík, M.; Etrych, T.; Bakkour, Y.; Coudane, J.; El Omar, F.; Nottelet, B. PCL-PEG Graft Copolymers with Tunable Amphiphilicity as Efficient Drug Delivery Systems. *J. Mater. Chem. B* **2016**, *4* (37), 6228–6239. <https://doi.org/10.1039/C6TB01841F>.
- (17) Chu, B.; Zhang, L.; Qu, Y.; Chen, X.; Peng, J.; Huang, Y.; Qian, Z. Synthesis, Characterization and Drug Loading Property of Monomethoxy-Poly(Ethylene Glycol)-Poly(ε-Caprolactone)-Poly(D,L-Lactide) (MPEG-PCLA) Copolymers. *Sci. Rep.* **2016**, *6* (1). <https://doi.org/10.1038/srep34069>.
- (18) Shi, Y.; Ma, W.; Gao, M.; Yang, Y. Development of Curcumin-Loaded Methoxy Poly(Ethylene Glycol)-Block-Poly(Caprolactone)-Block-Poly(1, 4, 8-Trioxa [4.6] Spiro-9-Undecanone) Nanoparticles and Studies on Their in Vitro Anti-Tumor Activities. *Colloids Surf. B Biointerfaces* **2019**, *184*, 110525. <https://doi.org/10.1016/j.colsurfb.2019.110525>.
- (19) Lu, C.; Guo, S.; Zhang, Y.; Yin, M. Synthesis and Aggregation Behavior of Four Types of Different Shaped PCL-PEG Block

Copolymers. *Polym. Int.* **2006**, *55* (6), 694–700. <https://doi.org/10.1002/pi.2034>.

(20) Surnar, B.; Jayakannan, M. Structural Engineering of Biodegradable PCL Block Copolymer Nanoassemblies for Enzyme-Controlled Drug Delivery in Cancer Cells. *ACS Biomater. Sci. Eng.* **2016**, *2* (11), 1926–1941. <https://doi.org/10.1021/acsbiomaterials.6b00310>.

(21) Toncheva-Moncheva, N.; Bakardzhiev, P.; Rangelov, S.; Trzebicka, B.; Forsys, A.; Petrov, P. D. Linear Amphiphilic Polyglycidol/Poly(ϵ -Caprolactone) Block Copolymers Prepared via “Click” Chemistry-Based Concept. *Macromolecules* **2019**, *52* (9), 3435–3447. <https://doi.org/10.1021/acs.macromol.9b00366>.

(22) Celentano, W.; Ordanini, S.; Bruni, R.; Marocco, L.; Medaglia, P.; Rossi, A.; Buzzaccaro, S.; Cellesi, F. Complex Poly(ϵ -Caprolactone)/Poly(Ethylene Glycol) Copolymer Architectures and Their Effects on Nanoparticle Self-Assembly and Drug Nanoencapsulation. *Eur. Polym. J.* **2021**, *144*, 110226. <https://doi.org/10.1016/j.eurpolymj.2020.110226>.

(23) Mou, L.; Chen, N.; Zhu, K.; Chen, Y.; Luo, X. Copolymer of Star Poly(Epsilon-Caprolactone) and Polyglycidols as Potential Carriers for Hydrophobic Drugs. *Polym. Adv. Technol.* **2012**, *23* (4), 748–755. <https://doi.org/10.1002/pat.1952>.

(24) Zhang, X.; Cheng, J.; Zhuo, R. Amphiphilic Hyperbranched Polymers with a Biodegradable Hyperbranched Poly(ϵ -Caprolactone) Core Prepared from Homologous AB₂ Macromonomer. *RSC Adv.* **2016**, *6* (57), 52334–52338. <https://doi.org/10.1039/C6RA08531H>.

(25) Yang, H.-K. Bioreducible Amphiphilic Block Copolymers Based on PCL and Glycopolypeptide as Multifunctional Theranostic Nanocarriers for Drug Delivery and MR Imaging. *RSC Adv.* **2017**, *7*, 21093–21106.

(26) Delorme, V.; Lichon, L.; Mahindad, H.; Hunger, S.; Laroui, N.; Daurat, M.; Godefroy, A.; Coudane, J.; Gary-Bobo, M.; Van Den Berghe, H. Reverse Poly(ϵ -Caprolactone)-g-Dextran Graft Copolymers. Nano-Carriers for Intracellular Uptake of Anticancer Drugs. *Carbohydr. Polym.* **2020**, *232*, 115764. <https://doi.org/10.1016/j.carbpol.2019.115764>.

(27) Reisch, A.; Klymchenko, A. S. Fluorescent Polymer Nanoparticles Based on Dyes: Seeking Brighter Tools for Bioimaging. *Small* **2016**, *12* (15), 1968–1992. <https://doi.org/10.1002/sml.201503396>.

(28) Khalin, I.; Heimbürger, D.; Melnychuk, N.; Collot, M.; Groschup, B.; Hellal, F.; Reisch, A.; Plesnila, N.; Klymchenko, A. S. Ultrabright Fluorescent Polymeric Nanoparticles with a Stealth Pluronic Shell for Live Tracking in the Mouse Brain. *ACS Nano* **2020**, *14* (8), 9755–9770. <https://doi.org/10.1021/acsnano.0c01505>.

(29) Bou, S.; Klymchenko, A. S.; Collot, M. Fluorescent Labeling of Biocompatible Block Copolymers: Synthetic Strategies and Applications in Bioimaging. *Mater. Adv.* **2021**. <https://doi.org/10.1039/D1MA00110H>.

(30) Bou, S.; Wang, X.; Anton, N.; Bouchaala, R.; Klymchenko, A. S.; Collot, M. Lipid-Core/Polymer-Shell Hybrid Nanoparticles: Synthesis and Characterization by Fluorescence Labeling and Electrophoresis. *Soft Matter* **2020**, *16* (17), 4173–4181. <https://doi.org/10.1039/D0SM00077A>.

(31) Klymchenko, A. S. Solvatochromic and Fluorogenic Dyes as Environment-Sensitive Probes: Design and Biological Applications. *Acc. Chem. Res.* **2017**, *50* (2), 366–375.

<https://doi.org/10.1021/acs.accounts.6b00517>.

(32) Bao, Y.; De Keersmaecker, H.; Corneillie, S.; Yu, F.; Mizuno, H.; Zhang, G.; Hofkens, J.; Mendrek, B.; Kowalczyk, A.; Smet, M. Tunable Ratiometric Fluorescence Sensing of Intracellular PH by Aggregation-Induced Emission-Active Hyperbranched Polymer Nanoparticles. *Chem. Mater.* **2015**, *27* (9), 3450–3455. <https://doi.org/10.1021/acs.chemmater.5b00858>.

(33) Kulkarni, B.; Malhotra, M.; Jayakannan, M. Perylene-Tagged Polycaprolactone Block Copolymers and Their Enzyme-Biodegradable Fluorescent Nanoassemblies for Intracellular Bio-Imaging in Cancer Cells. *ACS Appl. Polym. Mater.* **2019**, *1* (12), 3375–3388. <https://doi.org/10.1021/acsapm.9b00800>.

(34) Trofymchuk, K.; Valanciunaite, J.; Andreiuk, B.; Reisch, A.; Collot, M.; Klymchenko, A. S. BODIPY-Loaded Polymer Nanoparticles: Chemical Structure of Cargo Defines Leakage from Nanocarrier in Living Cells. *J. Mater. Chem. B* **2019**, *7* (34), 5199–5210. <https://doi.org/10.1039/C8TB02781A>.

(35) Fuhrmann, K.; Gauthier, M. A.; Leroux, J.-C. Crosslinkable Polymers for Nanocrystal Stabilization. *J. Controlled Release* **2010**, *148* (1), e12–e13. <https://doi.org/10.1016/j.jconrel.2010.07.006>.

(36) Lee, K. W.; Chung, J. W.; Kwak, S.-Y. Highly Branched Polycaprolactone/Glycidol Copolymeric Green Plasticizer by One-Pot Solvent-Free Polymerization. *ACS Sustain. Chem. Eng.* **2018**, *6* (7), 9006–9017. <https://doi.org/10.1021/acssuschemeng.8b01356>.

(37) Collot, M.; Fam, T. K.; Ashokkumar, P.; Faklaris, O.; Galli, T.; Danglot, L.; Klymchenko, A. S. Ultrabright and Fluorogenic Probes for Multicolor Imaging and Tracking of Lipid Droplets in Cells and Tissues. *J. Am. Chem. Soc.* **2018**, *140* (16), 5401–5411. <https://doi.org/10.1021/jacs.7b12817>.

(38) Postma, A.; Davis, T. P.; Donovan, A. R.; Li, G.; Moad, G.; Mulder, R.; O’Shea, M. S. A Simple Method for Determining Protic End-Groups of Synthetic Polymers by ¹H NMR Spectroscopy. *Polymer* **2006**, *47* (6), 1899–1911. <https://doi.org/10.1016/j.polymer.2006.01.050>.

(39) Nguyen, T. Q. Liquid chromatography of synthetic polymers: Principles and applications (in French). *Analisis* **1998**, *26* (2), 35–41. <https://doi.org/10.1051/analisis:199826020035>.

(40) Targeted Solvatochromic Fluorescent Probes for Imaging Lipid Order in Organelles under Oxidative and Mechanical Stress | Journal of the American Chemical Society <https://pubs-acsc-org.scd-rproxy.u-strasbg.fr/doi/10.1021/jacs.0c10972> (accessed 2021-07-16).

(41) Wang, X.; Collot, M.; Omran, Z.; Vandamme, T. F.; Klymchenko, A.; Anton, N. Further Insights into Release Mechanisms from Nano-Emulsions, Assessed by a Simple Fluorescence-Based Method. *J. Colloid Interface Sci.* **2020**, *578*, 768–778. <https://doi.org/10.1016/j.jcis.2020.06.028>.

(42) Kurniasih, I. N.; Liang, H.; Mohr, P. C.; Khot, G.; Rabe, J. P.; Mohr, A. Nile Red Dye in Aqueous Surfactant and Micellar Solution. *Langmuir* **2015**, *31* (9), 2639–2648. <https://doi.org/10.1021/la504378m>.

(43) Collot, M.; Schild, J.; Fam, K. T.; Bouchaala, R.; Klymchenko, A. S. Stealth and Bright Monomolecular Fluorescent Organic Nanoparticles Based on Folded Amphiphilic Polymer. *ACS Nano* **2020**. <https://doi.org/10.1021/acsnano.0c06348>.

(44) Monopoli, M. P.; Åberg, C.; Salvati, A.; Dawson, K. A. Biomolecular Coronas Provide the Biological Identity of Nanosized

Materials. *Nat. Nanotechnol.* **2012**, *7* (12), 779–786. <https://doi.org/10.1038/nnano.2012.207>.

(45) Ke, P. C.; Lin, S.; Parak, W. J.; Davis, T. P.; Caruso, F. A Decade of the Protein Corona. *ACS Nano* **2017**, *11* (12), 11773–11776. <https://doi.org/10.1021/acsnano.7b08008>.

(46) Darwich, Z.; Klymchenko, A. S.; Dujardin, D.; Mély, Y. Imaging Lipid Order Changes in Endosome Membranes of Live Cells by Using a Nile Red-Based Membrane Probe. *RSC Adv.* **2014**, *4* (17), 8481–8488. <https://doi.org/10.1039/C3RA47181K>.

(47) Wu, L.; Huang, C.; Emery, B. P.; Sedgwick, A. C.; Bull, S. D.; He, X.-P.; Tian, H.; Yoon, J.; Sessler, J. L.; James, T. D. Förster Resonance Energy Transfer (FRET)-Based Small-Molecule Sensors and Imaging Agents. *Chem. Soc. Rev.* **2020**, *49* (15), 5110–5139. <https://doi.org/10.1039/C9CS00318E>.

(48) Mukherjee, T.; Kanvah, S.; Klymchenko, A. S.; Collot, M.

Probing Variations of Reduction Activity at the Plasma Membrane Using a Targeted Ratiometric FRET Probe. *ACS Appl. Mater. Interfaces* **2021**, *13* (34), 40315–40324. <https://doi.org/10.1021/acsaami.1c11069>.

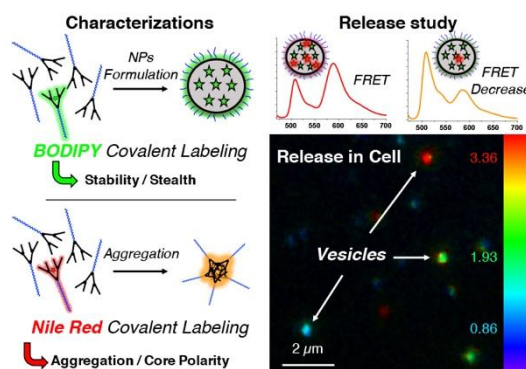
(49) Reisch, A.; Didier, P.; Richert, L.; Oncul, S.; Arntz, Y.; Mély, Y.; Klymchenko, A. S. Collective Fluorescence Switching of Counterion-Assembled Dyes in Polymer Nanoparticles. *Nat. Commun.* **2014**, *5* (1), 4089. <https://doi.org/10.1038/ncomms5089>.

(50) Andreiuk, B.; Reisch, A.; Bernhardt, E.; Klymchenko, A. S. Fighting Aggregation-Caused Quenching and Leakage of Dyes in Fluorescent Polymer Nanoparticles: Universal Role of Counterion. *Chem. – Asian J.* **2019**, *14* (6), 836–846. <https://doi.org/10.1002/asia.201801592>.

Table of content:

Fluorescent Labeling of Branched Copolymers: a Method for *In Situ* Characterization of Nanovectors and Imaging of Cargo Release

Sophie Bou,¹ Andrey S. Klymchenko,¹ Mayeul Collot^{1*}



Covalent labeling of PEG-PCL branched copolymers with BODIPY or environment sensitive Nile Red fluorophores allowed in depth characterizations (stability, stealth, aggregation, core polarity) of the formulated nanoparticles using spectroscopic techniques and enabled to monitor their cargo release in cells using FRET and ratiometric imaging.